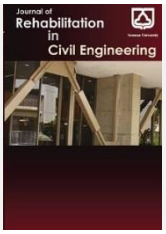

Journal of Rehabilitation in Civil Engineering

Journal homepage: https://civiljournal.semnan.ac.ir/

Behaviour of Reinforced Self-Compacted Layered-Concrete Deep Beams under Monotonic Loading

Qasim M. Shakir [1*]; Hawraa K. Hannon [1]

1. Department of Civil Engineering, Faculty of Engineering, University of Kufa, Najaf, Iraq

* Corresponding author: *qasimm.alabbasi@uokufa.edu.iq*

ARTICLE INFO

Article history:
Received: 04 April 2024
Revised: 16 January 2025
Accepted: 17 January 2025

Keywords:
Layered deep beams;
Steel fiber concrete;
Reactive powder concrete;
Shear span effect;
Flexural toughness.

ABSTRACT

The use of reinforced concrete (RC) deep beams has expanded dramatically over the past few decades. Then, improving the performance while maintaining the cost as low as possible cost has become a critical concern. In the current work, a layered model based on using high performance concrete (HPC) at the top half of the section only has been considered. Six specimens were tested experimentally under static load up to failure. It is aimed to determine the range of improvement in the general performance due to use of steel fiber concrete (SFC) or reactive power concrete (RPC) at the top half of the deep beams. Moreover, the effect of loading configuration (one-point or two points) which considered implicitly the effect of the shear span-to- depth ratio (a/h) was considered. The response was studied in terms of several indicators including the load-deflection curve, the failure load the crack width, the mode of failure, map of cracking, toughness, and ductility. Results showed that for one-point load, the failure loads for the hybrid specimens with SFC and RPC at top layers of the section was enhanced by 22% and 28% relative to the non-hybrid model. While enhancements of 27% and 34% were recorded under two point loads. Moreover, it was found that reducing a/d ration from 1.67 to 1.22 resulted in enhancements of 32%, 37% and 39% for the non-hybrid and hybrid sections respectively. Regarding toughness, enhancements of 28% and 144%, were obtained for the specimens hybrid with SFC under one-point and two-point loading systems respectively. When RPC was used, the corresponding improvements were 44% and 188%, respectively.

E-ISSN: 2345-4423

How to cite this article:
Shakir, Q. M. and Hannon, H. K. (2026). Behaviour of Reinforced Self-Compacted Layered-Concrete Deep Beams under Monotonic Loading. Journal of Rehabilitation in Civil Engineering, 14(1), 2037 https://doi.org/10.22075/jrce.2024.33697.2037

1. Introduction

A deep beam under concentrated load is defined by the ACI318-19 code as one that, for simply supported beams, has a shear span to overall depth ratio of less than 2.0. Conversely, for a continuous beam, less than 2.5[1]. The classical theory of bending, or Bernoulli, cannot be used to design deep beams because it takes the section as constant before and after bending, ignoring shear deformations and concentrated stresses.[2]. Several techniques have been put forth, such as the method of shear friction [3] and the strut and tie modelling (STM) [1], In deep beams , the high ratio of shear/bending moment may results in a significant disturbance of the non-linear strain distribution. Corbels, piling caps, dapped end beams, connections, opening areas, and deep beams comprise the disturbed zone, also known as the D-region. Many applications for deep beams include pile caps, foundation walls, tank walls, high-rise buildings, and bridges [4].

Many studies were published in deep beams, Dang et.al. [5] reported that the failure mode is influenced by a/h. Smarzewski [6] concentrated on how response was affected by the a/d ratio and horizontal shear reinforcement. Patil 2013 [7] concluded that the main failure of deep beams was diagonal cracking. Zhang, et al. 2020 [8] found that the failure mode of deep beams with small a/d was diagonal compression failure, which is affected by shear reinforcement. Furthermore, the capacity of shear resistance improved with decreasing of a/d and increasing longitudinal reinforcement. Cailong , et al. 2021 [9] concluded that by increasing a/d ratio, the ultimate shear strength decreases.

Previous studies referred that the behavior of deep beams is affected by strength of concrete. Accordingly, steel fibers were incorporated to improve the strength of concrete [10], [11]. Steel fibers were used in various applications in deep beams. Several variables were considered including steel fibers ratio and a/d ratio. It was reported that some area of stirrups could be substituted by enough quantity of steel fibers and the flexural and shear capacities are affected by the proportion of steel fibers. Benard, et al. 2017[12] concluded that using the steel fibers enhanced the fatigue resistance, and reduced the deformation of the deep beam. Sergio, et al. 2021 [13] reported that, using higher ratios of steel fibers resulted in considerable enhancement in the resistance to shear cracks and the increasing the shear loading capacity (up to 30% and 55%) respectively and reduced the average crack width up to 44%. Manharawy et.al [14] studied light-weight deep beams with steel fibers. Saga et. al. [15] studied the effect of the ratio of fibers and type of loading on behavior of deep beams. Concha et.al. [16] proposed a model to predict shear strength considering various parameters. A hybrid neuro-swarm model was adopted and validated against previous studies. It was reported that the mode failure changed by adding steel fibers and takes the form of diagonal and vertical cracks. Hussain et. al. [17] investigated the response of UHPC deep beams including hybrid combination of steel and basalt fibers. .Several studies used the high performance concrete [18], [19], others used reactive powder concrete (RPC) in deep beams. Regarding RPC, Hani, et al. 2013 [20] tested specimens having strength under compression of (95-111)MPa. It was concluded that when the shear span –to- effective depth (a/d) ratio was decreased from 1.5 to 1.25 and 1, the resistance capacity to shear enhanced by 24.4% and 31.7%, respectively. In 2018 Mohammed and Mushriq [21]considered adding air bubbles (to reduce cost and weight) represented by plastic balls in the lower half of the section with a/d equal (1.11 and 1.67). The application of bubbles led to maximum weight and capacity reductions of 26% and 22%, respectively, according to the results. Fathi, et al. 2018 [22]tested RPC deep beams with square openings. Results showed that capcity reduced in a range (16%-93%) with opening sizes in range of (50-250)mm. Saad, et al. 2018 [23] examined how RPC deep beams with openings responded to repeated and monotonous loads. The findings showed that the ultimate load was reduced by 23.3%, 22.8%, and 2.6%, respectively, when the opening size is increased from 40 mm to 80 mm.

It is to be mentioned that cost of RPC restricted adopting such proposal widely. Thus, The hybrid modes were suggested considering at least one of the following three factors: cost, weight, and sustainability. Hassan 2014 [24] suggested dividing the bottom layer into RPC and the top layer into NSC (with contents of 0%, 0.5%, 1%). The bottom layer's steel fiber ratio was found to increase from 0% to 1%, which significantly improved the cracking load, ultimate load, and cracking map. Hassan and Faroun, 2016 [25] examined how the hybrid deep beams responded to a repeated, monotonous load. Normal concrete was placed in the center, and the shear span area was filled with fibrous concrete. The conclusion was that the beam had a 1% SF and was fully cast with SFC. The final load was 10.96% higher than with the hybrid beam. Ma, et al. 2018 [26] The behavior of the hybrid fiber deep beams was experimentally investigated by adding two types of steel fibers for the long/short (L/S) fibers in different ratios: 0%/0%, 0.75%/0.25%, and 1.5%/0.5%. Compared to the typical (0%/0% and no shear reinforcement) deep beam, it was discovered that the failure load enhanced by 67% and 114% when the two combinations of fiber were used, with 6#8 mm horizontal shear reinforcement and #8@200 vertical stirrups, respectively. Mhalhal, et al. 2020 [27] combine vertical and horizontal shear reinforcement (8#5mm) (closed stirrups/out of plane plates/in plane plates). Conclusion: Compared to the reference beam (which had the same horizontal shear reinforcement and closed stirrups), the crack and failure loads increased by (16–60)% and (15–19)%, respectively, and the mode of failure ranged in diagonal splitting–shear compression. Sada and Resan 2021 [28] examined two-layered deep beams with a trapezoidal section, concrete strengths of 25, 50, and 70 MPa, and side angles of 75, 80, and 85 degrees. The highest value of first crack resistance was found in a trapezoid cross-section having a side angle of 80^{o} and a compressive strength ratio of 0.5 and 0.357 for the bottom and top, respectively.

Recently, Shakir and Hannon [29], [30],[31] conducted a series of studies on which several models of hybrid models proposed aiming to produce precast deep beams with the least cost/weight without severe drop in performance. Several combinations of SFC, RPC, normal strength concrete (NSC) and light weight concrete (LWC) were used which are follows: SFC/NSC, RPC/NSC, SFC/LWC, and RPC/LWC. Then, the project was improved by Shakir and Alghazali in successive studies [32],[33],[34] to take sustainability into account. Three replacement ratios of recycled concrete (0%, 50%, and 100%) were utilized in place of crushed concrete. Because of the concrete type casing procedure, these suggested models can be used in precast applications; however, they might not be suitable for use with cast-in-place deep beams. Next, the layered model that could be applied to precast and cast-in-place models in production was examined in this study. NSC was used for the bottom layer and SFC or RPC for the top layer. The behavior has been examined in relation to dissipated energy, ductility, loading history, crack widening, failure load, and mode of failure.

2. Materials and methods

2.1. Detailing of the tested specimens

Six concrete deep beams measuring 450 mm in total depth, 180 mm in width, and 1700 mm in length. Each two beams have the same internal concrete type(s) and detailing, one was tested under a mid-span point (one-point) load with a/h= 1.67 and the other was tested under a two-point loads with a/h=1.2. The specimens are grouped according to the concrete types into three sets: the first set represented the control beams (CTRL-1P and CTRL-2P). The second set represents the hybrid specimens composed partially with SFC (G1-SN-1P and G1-SN-2P). While the third one included the specimens composed with RPC (G1-RN-1P and G1-RN-2P).

The STM simulation [1] served as the basis for the design of the steel reinforcement, which came in three sizes as illustrated in Fig. (2): bars of 8mm diameter with spacing of 130mm C/C as stirrups, two bars of

10 mm at the top of the beam, and three bars of 16 mm at the tensile steel (tie reinforcement). Normal strength concrete (NSC) is used to create two specimens; the upper half is composed of fibrous concrete (SFC), while the bottom layer is NSC. On the other hand, the other layers are composed of NSC at the bottom and reactive powder concrete (RPC) at the top. The characteristics of the deep beam specimens are indicated in Table 1.

Fig. 1. Detailing of steel reinforcement of the tested specimens.

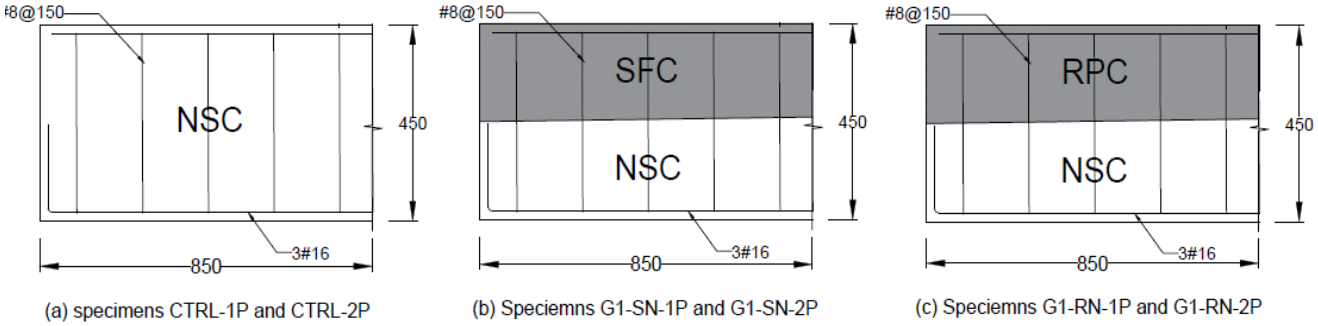

Fig. 2. Details of deep beams (one-half of the beams).

2.2. Material of the concrete mixes

In the experimental work, Ordinary Portland Cement (OPC) has been used. It was tested to meet Iraqi specification No. 5 from 1984. The washed natural sand was tested according Iraqi specifications, IQ.S No. 45/1984 and used in the steel fiber and regular concrete mixtures. Sand of high silica with particles of maximum size of 0.6 mm that was produced by AL-Nawafith Company in AL-Najaf was used as aggregate in the RPC mix. The standard concrete mix contained natural crushed gravel (19 mm), which had a clean, dry surface that was saturated. Crushed gravel with a maximum size of 14 mm was utilized in the mix of fibrous concrete (SFC).

The surface was dry and clean, meeting Iraqi specification No. 45/1984 in the process. An excellent fine mineral admixture for concrete, silica fume has been used in reactive powder concrete mixes. The goal of using micro steel fiber length /diameter ratio or aspect ratio (L/D) of (13.1/0.22) mm and tensile strength of 3005 N/mm^2 is to increase the shear resistance and durability of the mixes of the steel fiber and reactive powder concrete. There have been three distinct steel reinforcement sizes utilized. Bars of ten millimeters diameters are utilized as compression steel at the compression face and eight millimeters are used as shear reinforcement. 16 mm bars served as the maim bottom reinforcement. The yield stress/ ultimate strengths (in N/mm^2) and were, respectively, 445/630, 480/695, and 600/697. The mixture is self-compacting and has a lower water percentage thanks to the use of Master Glenium54. It also produces concrete mixes of high compressive strength with few voids and high workability without segregation of ingredients or bleeding of mix water. Lime stone, a finely crushed white powder is used to increase

content of fines in the mix of the self-consolidating concrete and improve workability in addition to the superplasticizer. Table (1) show the proportions of the constituent materials for the three mixes used in the present work.

2.3. Concrete mix properties

The self-compacting concrete was tested using the T500 Tests (Fig. 3a) and Slump Flow Tests, which are used to measure the flowability of the concrete mix. Self-compacting concrete (SCC) is tested for passing ability using the "J-Ring, Fig. (3b,c)." In terms of the mechanical characteristics, Cubes measuring 100 x 100 x 100 mm, cylinders measuring 100 mm in diameter and 200 mm in length, and cylinders measuring 150 mm in diameter and 300 mm in length were used to test the compressive strength, splitting tensile strength, and modulus of elasticity, respectively.

Table 1. Proportions for mix types used in the study.

Material	NSC	SFC	RPC
Cement (kg/m3)	470	517	900
Silica sand (kg/m3)	----	----	900
Sand (kg/m3)	837	600	-----
Gravel(max. 20 mm) (kg/m3)	800		-----
Gravel(max. 14 mm) (kg/m3)	---	1122	-----
Lime stone %Wt of cement	21		-----
Silica fume %(wt of cement)	----	---	25
Steel fiber (volume ratio)%	-----	1.5	1.5
Water (W/Binder%)	28	20.3	22.5
Super plasticizer **%**(weight of binder.)	1.5	0.75	2.5

(a) T500 and Slump flow tests.

(b) J-ring test.

(c) Compressive strength. (d) splitting strength.

Fig. 3. Fresh and mechanical tests of concrete.

Figure (3) display the tests for the fresh and hardened concrete, respectively. Tables (2) and Table (3) show the test results of the fresh concrete (SCC for the NSC) and hardened concrete phase.

Table 2. Test results of the self-consolidating concrete.

Test	Results	Specification Limits
Slump Flow (mm) [35]	630	(450-760)
T500 (sec) [35]	3	(3-5)
J-ring.(mm) [36]	35	(25-50)

Table 3. Mechanical properties of hardened concrete.

Type of mix	Cube strength MPa (f_{cu})	Tensile strength MPa (f_t)	Elastic modulus GPa (E)
RPC	93	9.1	39.323
SFC	72	7.72	36.406
NSC	46	2.41	27.405

2.4. Devices and tools

As seen in figure (4 a), the vertical deflection of the tested specimens was measured at the midspan of the beam using a Linear Variable Differential Transformer device (LVDT). As depicted in figure (4 b), the measurement of the crack width was achieved using a crack meter with a 0.5 mm accuracy. A digital Vernia was used to measure the crack when its width was greater than 0.5 mm, as shown in Fig. (4c). The crack width was measured at 40kN intervals. The data of the applied loads and the corresponding deflections are recorded using a data logger device (Fig. 4d). The load-applying device is constructed with a robust steel base fastened to a concrete frame. It features a central hydraulic jack and piston. Each deep beam was tested under a monotonic static load that increased gradually up to failure. Each load increase was 5 kN. While, 20 kN increments are made after a 140 kN load until failure. With every increment, the readings were manually recorded. The progression of the crack is shown for each stage. Measurements are made of the crack width at each stage.

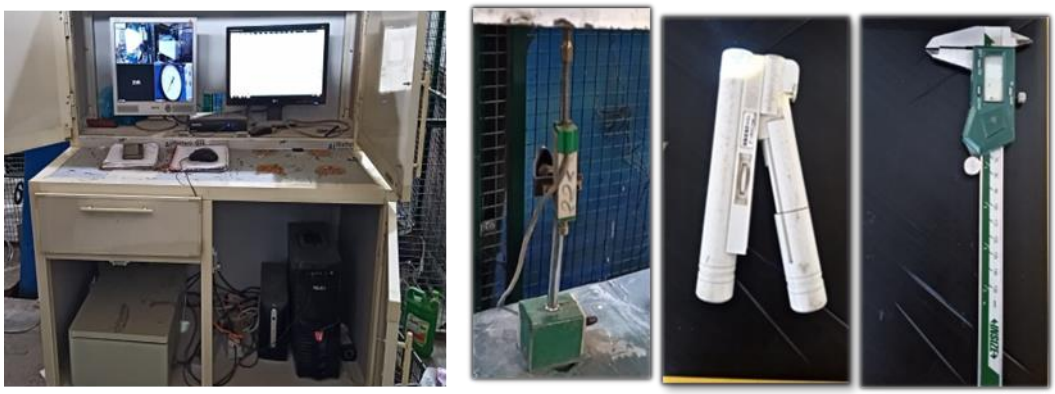

(a) Data logger (b) LVDT (c) crack meter (d) digital vernia

Fig. 4. Measuring devices and tools.

3. Results and discussion

3.1. Map of cracking

Figure (5a) displays the cracking map for the CTRL-2P control specimen. The first crack, as is customary, happened at mid span in the 80 kN pure B.M. region. Vertically oriented cracks appeared at the interaction of the regions of maximum bending moment (B.M.) and shear within a load level of 120 kN. Additional fissures propagated perpendicular to the supports along trajectories with progressively smaller angles. The diagonal crack with an angle of 41.5 degrees developed along the compression struts at a

loading level of 200 kN, traveling in the direction of the concentrated load at the top of the beam. Nonetheless, prior to failure, there was some crushing close to support.

At 400 kN of load, some horizontally oriented cracking at the compression face were noticed, indicating that concrete may have a tendency to spall if the load is distributed in a few concentrated areas. Following a diagonal cracking + spalling mode failure, the beam failure was noticed at a load level of 542 kN. Figure 5b, which depicts the specimen CTRL-1P's crack pattern, indicates that the initial crack began as a flexural type at midspan under a loading stage of 70 kN. This can be explained by the B.M. diagram's profile, which shows that the maximum value of the bending moment (PL/4) was induced at mid-span, as well as by the low tensile strength of the concrete at the bottom fiber.

As the load increased, the interacted regions between the decreased B.M. and the constant value of shear force (along the shear span) resulted in spreading cracks on both sides of the beam with the flatter orientation. The outermost diagonal crack that is suggested to link the point load and support reaction by an angle of 37 degrees occurs at 160 kN loading level. Given that the ductile mode of failure governed the behavior within the final stages of loading, it can be observed that this crack does not lie exactly within the strut paths. Additionally, cracks started to form closer to the compression face, which caused the compression block to gradually be weakened until load reached 410 kN, the point at which flexural failure happened. There hasn't been any noticeable crushing at the compression face. Therefore, it can be said that increasing the tensile steel will result in a higher capacity. It should be noted that some crushing happened at the support regions as a result of the stresses being concentrated there, which could have led to failure.

The specimen G1-SN-2P's cracking pattern is displayed in Figure (6a). With a load of 80kN, the first cracks developed at the region of maximum B.M. (in shallow beams, this area is controlled by flexural behavior) spread out on both sides of the beam which was controlled initially by flexural mode. More cracking occurred close to the supports without experiencing crushing, A diagonal crack, was initiated at 160 kN and inclined at an angle of 42^{o}. The mode of failure was vertical cracking that developed beneath the concentrated load when the loading reached 688 kN. Compared to control specimens CTRL-2P, it can be noticed that using the horizontal model of hybridization increased the deep beam's capacity by 26.9%. This could be explained by the fact that strengthening the compression block improved the flexural resistance. One possible factor in initialization of the mode of diagonal cracking is the comparatively short path to be followed between the two severely stressed regions i.e. the concentrated loads and support reactions. It should be noted that because of the relatively highly concentrated stresses, some crushing happened at the supports. This could lead to a decrease in capacity and the specimen failing before the section reaches its maximum capacity. Therefore, it is anticipated that greater capacity may be achieved if this failure localization is controlled.

The pattern of the crack propagation at the specimen G1-SN-1P's failure is depicted in Figure (6b). The initial crack developed as a flexural crack at the midspan at a load level of 80 kN. As the load increased, a vertical crack developed. The SF content in the top concrete slows the spread of cracks when they reach the layer of steel fiber concrete. As a result, more cracks with steep angles developed away from the flexural crack towards the supports.

Shear cracks move diagonally in the direction of the loading point. The formation of the diagonal cracks close to the lines as in the reference beams is restricted by the top layer's resistance to the penetration of cracks. As a result, the majority of the strain energy was released when the first flexural crack was initiated and ascended vertically to the loading point. Because of the problem of the stress concentration (D-regions), little crushing happened at the support reactions.

The flexural mode failure happened at a load of 460 kN. In contrast to the CTRL-1P reference specimens, the hybrid deep beam's capacity increased by 12.2%. It is possible to attribute the specimen's flexural mode of failure to the STM model that was adopted, which suggested a minimum amount (conservative) of steel area that interrupts the compression strut. This could cause the mode to change from being diagonally oriented to yield more ductility (flexure failure). Furthermore, it can be inferred that the simulation of STM mechanism computes tie reinforcement with less conservatism.

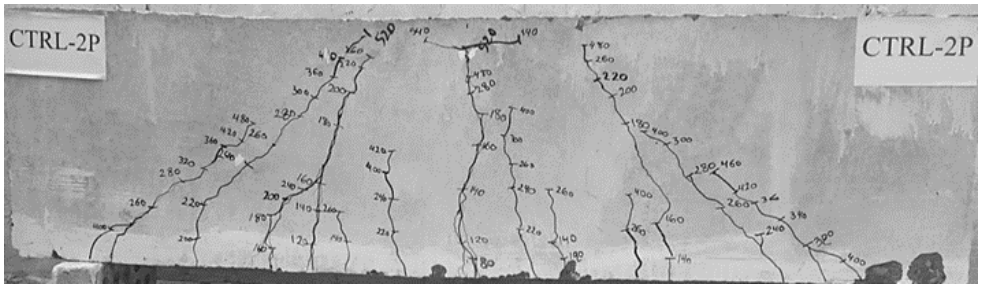

(a) Beam CTRL-2P.

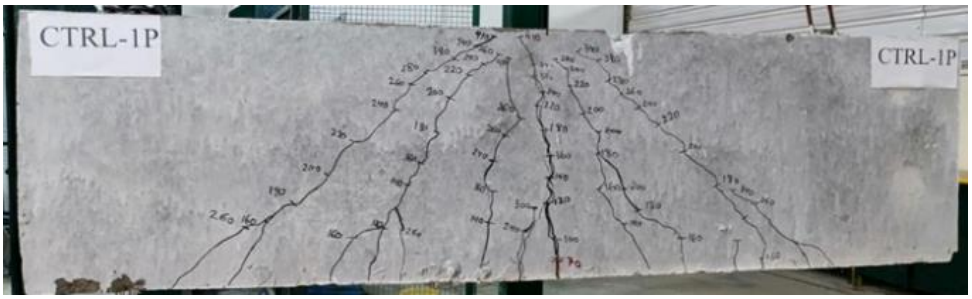

(b) Beam CTRL-1P.

Fig. 5. Crack patterns of the control specimens.

For specimen G1-RN-2P, the first flexural crack manifests in the maximum moment area at a load level of 80 kN, figure (6c). Subsequently, every crack propagates within the pure moment area and continues to grow upward, slowing down at the RPC. Because of the stronger struts region, the shear cracks propagated on sides and the main diagonal crack, developed with an angle of 50 ^{o}, which is more inclined than the CTRL-2P pattern, which has an angle of 42 ^{o}.

Some diagonal cracks appeared in the normal concrete layer near the supports after the load was increased beyond 300 kN. Because of the extreme concentration of stresses, crushing happens at the supports. The flexural-shear mode caused the failure at 727 kN. It is evident that with the strut areas improved, the deep beam's capacity is improved by 34.1% in comparison with the reference model.

Specimen G1-RN-1P and specimen G1-RN-2P share a hybridization model; the loading system is the only distinction. It is anticipated that the control specimen's failure resulted from the development of a flexural crack up with progress and loading, exhausting the axial force of the compression concrete block. As a result, the tension and compression forces' equilibrium was broken.

As a result, the prior hybrid deep beam model relied on using steel fibers to increase the energy required to cause the crack to propagate and raise the compression force of the compression block by increasing the concrete's compressive strength.

In this model, the top layer of concrete is made of reactive powder, and the bottom layer is made of normal strength concrete. Figure (6d) shows that at a load stage of 90 kN, the first cracking was noticed at

the mid span. Compared to steel fiber concrete, the development of this crack is more constrained when it reaches the top layer of concrete. As a result, additional cracks in the bottom layer appeared on both sides.

The curvature is limited, and the cracks propagate laterally at a slower rate than in the control specimen. This clarifies the reasons that, in specimen G1-RN-1P, the diagonal crack initiated at load 180 kN, but in the reference deep beam, it developed at load 160 kN. Failure happened at a load of 523 kN after a semi-diagonal mode of flexural-shear failure, resulting in a 27.6% increase in capacity over the reference specimen. Compared to G1-RN-2P, this model's deep beam capacity drops by 28%.

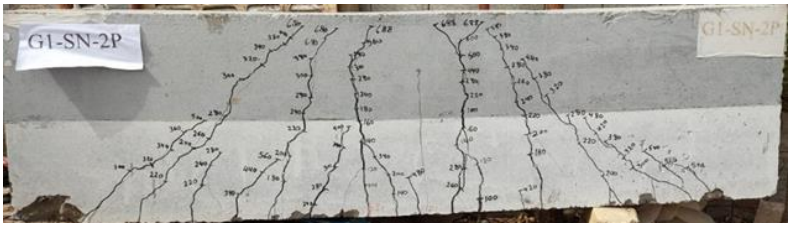

(a) Cracking map of the beam G1-SN-2P.

(b) Cracking map of the beam G1-SN-1P.

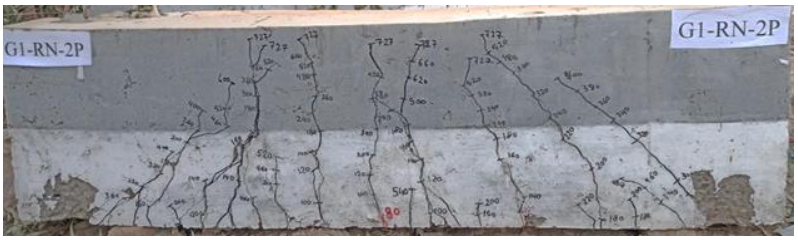

(c) Cracking map of the beam G1-RN-2P.

(d) Cracking map of the beam G1-RN-1P

Fig. 6. Crack Patterns of the layered Specimen.

3.2. Load –deflection curve

The load-deflection results for the deep beams specimens are displayed in Fig. (7). It is evident that the failure load and maximum deflection are significantly impacted by the loading system. i.e., greater load and deflection were produced by the distribution of loads across two points. This might be explained by the two-point system's decreased load concentration of stresses, which in turn prevented concrete from being crushed and improved the transfer of stresses to the supports.

There may be a substantial interaction between the maximum B.M. and maximum shear force for one point loading where a/d >1. Then, the level of stress could rise. If there is no interaction during two-point loading, then additional stresses may be accommodated until failure.

The disturbance of the transfer of stresses is relatively high for small values of (a/d) <1.0. Then, only D-regions are included in the deep beam. Compared to one-point loads, two-point loading results in shorter compression struts that could fail by splitting along them. Subsequently, the two-loading splitting range along the strut is decreased. In the current study, specimens tested under two-point loading showed increments of 32%, 37%, and 39 when compared to one point.

The STM model, which is an ideal truss made up of compression elements (struts), tie elements as steel reinforcements, and the connecting hinges—represented by nodal points—simulates the transfer of stresses in deep beams. Then, in order to continue resisting, all three components must be kept safe from failure. These failure modes include crushing of the nodal points, yielding of the tie elements, and spalling along the compression struts.

The inclined struts spall less under two-point loads than under one-point loads. However, there is a chance that the horizontal strut will fail between the top nodal point. Furthermore, one-point loads rather than two-point loads are more likely to cause crushing at the top nodal point.

In relation to the tie elements, Fig. 7 shows that the tensile force is equal to P/2 cot θ. Then, for the same beam dimensions, the angle (φ1) for a one-point load is smaller than the angle (φ2) for a two-point load. As a result, if there is no strut element spalling failure, more tensile load (P2 > P1) may be applied and more vertical load may be applied.

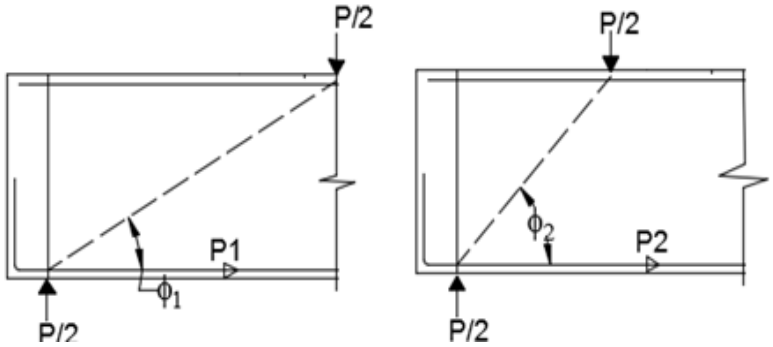

Fig 7. Effect of loading system on the tie force.

It may be observed that for the reference CTRL-2P specimen, the elastic stage terminated at a load of 460 kN, after which there was an abrupt change in stiffness as a result of the crack propagating. It is evident that a large amount of curvature and spalling within the compassion block occurred as a result of the pure bending moment within the mid-region (between loads) and the moderate amount of longitudinal steel. This premature failure and early test termination were caused by the relatively low strength of the concrete.

Using the SFC at the upper half, it is evident that there was no discernible difference at the elastic stage because steel fibers play the same role in both RPC and SFC in resisting and delaying the onset of cracking. By boosting strength and providing more tensile strength, SFC stopped the spalling. Furthermore, a portion of the struts composed of SFC that are unique to the lower layer will be used.

The tested group's maximum behavior limit is shown by the specimen G1-RN-2P's curve. Up to 510 kN, it is evident that the behavior is completely elastic. Past this point, there were some cracks that led to a decrease in stiffness because the main steel (bottom steel) was continuously elongating and the cracks

gradually spread throughout the deep beam's body. The stiffness decreased gradually until it failed at a load of 727 kN, with a maximum deflection of 24.5 mm.

Both curves, in particular G1-RN-2p, can be seen to have ended with stiffness=0.0.This indicates that the failure was ductile and that the compressive force at the compression block was not completely equilibrated by the tension force in the steel. It follows that raising the steel ratio should enhance the ductility, stiffness, and capacity.

The histories of loading for the specimens with SFC at the top layer and tested under one-point loading are displayed with that of Specimen CTRL-1P, Fig. 8. It is clear that the control specimen's load-deflection curve is composed of two linear segments around a load of 350 kN. The stiffness was initially maintained at 58 KN/mm up to 340 kN, after which it changed to 16 kN/mm and remained constant until failure.

The uniformity of the stress transfer from concrete to steel and the rate of cracking are indicated by the constant stiffness values observed through the two points at 380 kN. After that, the stiffness somewhat decreased at a faster rate. After that, it was maintained at a constant 16 kN/mm value until it failed. This might be because one of the flexural cracks at the midspan dominates and controls behavior all the way to failure.

As with the control specimen, the specimen G1-SN-1P's initial stiffness was maintained at 65 kN/mm throughout its entire length. Beyond that, the bottom NSC layer began to gradually lose stiffness as a result of the cracks propagating through it. This rate of loss is maintained constant until the failure, which happens at level 503 kN at the bottom layer, is reached.

The loading history of the specimen G1-RN-1P tested under a concentrated loading system for RPC specimens is displayed in figure. Because the RPC is located at the top of the beam, it is evident that the initial stiffness of the majority of specimens is higher than that of the control specimen. The hybrid deep beam that was horizontal in shape yielded slightly less stiffness than the control sample. Nonetheless, the stiffness is kept constant up to a load range that is 29% higher than that of the control specimen.

This could be explained by the steel fibers in the top portion of the compression strut, which prevented the rate of cracking from increasing under heavier loads. After that, the stiffness decreased by 81% to a steady 10.5 kN/mm. At this point, the specimen could support an additional load, or 16% of the total load. The experimental test records for the tested specimens are displayed in Table (4).

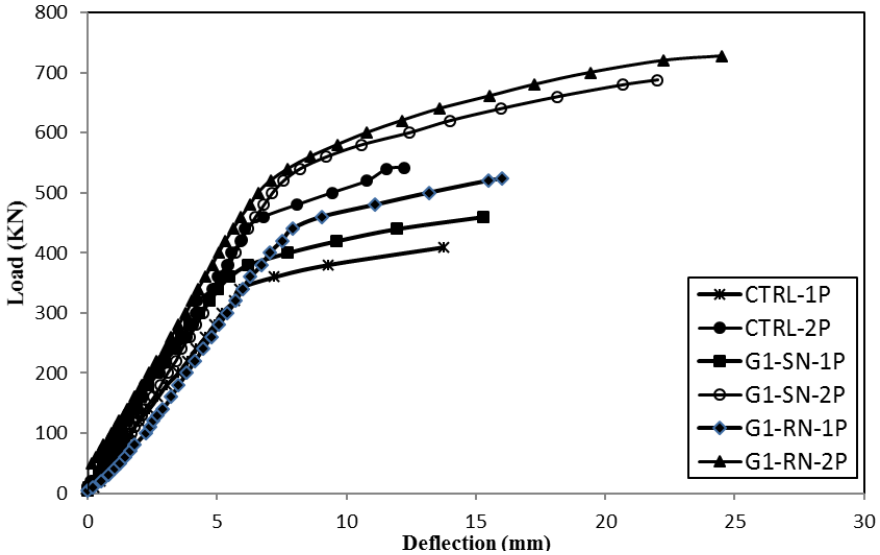

Fig 8. load deflection curve

3.3 Cracking width

The rate at which the flexural cracks have been widened during loading regimes are depicted in Fig. (9a). It is evident that models tested under one-point loading exhibited much greater crack widening than specimens tested under two points loads. Furthermore, the outcomes demonstrated that under one-point loading, the cracking limits are comparable. This can be explained by the fact that additional loading caused additional cracks to initiate and the initial crack's width to increase after it was first initiated at the midspan (max. mom).

However, the rate that the flexural crack widened was higher than the diagonal one due to the improved cracking resistance of the top layer (steel fiber concrete or reactive powder concrete), the longer compression struts that cross more stirrups than those for two-point loading, and the location of the maximum moment at mid-span.

Table (4) Results of the tested deep beam specimens

Specimens	Pcr	Pu (kN)	max (mm)	Width of crack (mm)
CTRL-1P	70	410	13.76	3.05
CTRL-2P	80	542	12.24	2.64
G1-SN-2P	80	688	22.02	1.45
G1-SN-1P	80	503	15.44	3.5
G1-RN-2P	80	727	24.49	2.12
G1-RN-1P	90	523	16.07	3.47

Additionally, it can be seen that, for specimens subjected to a single point load, the variation in crack width was only 3–3.5 mm, whereas for hybrid specimens, the crack reached 1 mm at the same loads. There is no discernible difference in the results when either of the two concretes is used to create the two layers.

It is evident that under two-point loading, the values for specimen CTRL-1P and control specimen CTRL-2P are extremely similar. However, there is a noticeable difference with the hybrid beams. This is because the steel fiber concrete provides sufficient strength to balance the tensile force developed in the main steel, and the higher strength of the concrete combined with the effect of bridging the fibers (SF) resulted in significant enhancement in rigidity and restraint the excessive widening of the flexural crack.

Moreover, the STM model indicated that stress transfer does not primarily occur in the midspan region. On the other hand, tie elements (steel bars) transfer the tension forces, and compression struts transfer the compressive forces. When these forces come together at the modal points, they ought to fulfill the equilibrium condition. Once more, it is evident that using SFC instead on RPC yielded no discernible difference in behavior.

The diagonal crack width's evolution with loading progress is depicted in Fig. (9b). It is evident that specimens tested under one concentrated load exhibit less crack widening than specimens tested under two-point loads, and that the diagonal crack reaches a point of stagnation at failure in contrast to two-point loading, where the widening is unbounded.

In contrast to the other two specimens, the specimen CTRL-1P's diagonal crack, however, appears to have produced a comparatively higher rate of widening. This figure shows that flexure caused the specimen with a single point of loading to fail. In terms of the two-point load, specimens with SFC and RPC failed

by flexure, whereas specimen CTRL-2P failed due to an interaction between the flexural and diagonal modes. This finding suggests that the failure was ductile and that adding more steel bars to the bottom could increase resistance.

There is a large enough range for the mode of failure to shift to the diagonal mode. The results also show that decreasing the degree of load distribution in the load configuration results in a corresponding decrease in capacity. It is possible to achieve a safer mode of failure. It should be noted that the behavior of the deep beams can be improved with the right strengthening technique. It is evident that applying the concentrated load in two locations as opposed to one improved loading transfer to the supports and reduced stress concentration, preventing local failure.

Furthermore, the rate of crack widening appears to be small compared with those of the specimens tested under one point loading. When the flexure and diagonal shear cracks were compared for the CTRL-1P control specimen, they both grew uniformly and at a similar rate until a 300 kN load was applied. The diagonal cracked 1.1 mm, whereas the flexure crack increased in widening and become the controlling crack recording a width of 3.05 mm close to failure stage. This could be explained by the stirrups interrupting the diagonal lines, which helped to stabilize the diagonal cracking. This indicates that the flexural mode was the cause of the failure.

At 80 kN of load, vertical cracks at midspan (flexural type) of the G1-SN-1P specimen initially manifested. At 180 kN, the diagonal cracks then started to develop. Up to a load of 220 kN, the rates of widening of the two types of cracks were in balance. Following that, the diagonal crack is slowed down when it reaches the steel fiber SFC layer, which causes the flexural crack to start developing quickly. The upward vertical crack grows toward the loading point and takes center stage, expanding to a width of 3.5 mm at failure, while the diagonal shear cracks measure 0.45 mm. A 59% decrease in diagonal crack width at failure compared to the control beam as a result of the top layer of the beam containing SFC. Furthermore, the avoidance of local failure was achieved through improved loading transfer and stress distribution on the beam.

Additionally, it is evident that enhancing the hybrid model decreased the diagonal crack's rate of widening while having less of an impact on the flexural crack. Because the strength of the compression block and the quantity of tension steel control this kind of crack.

It is evident that the diagonal flexural crack is widening at a slower rate than the G1-RN-1P one. This could be explained by the STM model that suggests utilizing a minimum value for the steel that crosses the compression strut. When more steel is used than the minimum amount, it may shift the behavior to be dominated by flexural failure.

Additionally, the results demonstrate that the reference specimen's rate of widening for both types of cracks is more than the G1-RN-1P specimen's, which may be related to the impact of the RPC that was used. When comparing Figures 4-30 and 4-32, it is evident that the specimens included in RPC exhibit a slower rate of diagonal crack widening than the specimens included in SFC. Even though there is less of an impact on flexural cracks, this is because RPC has a stronger strength than SFC.

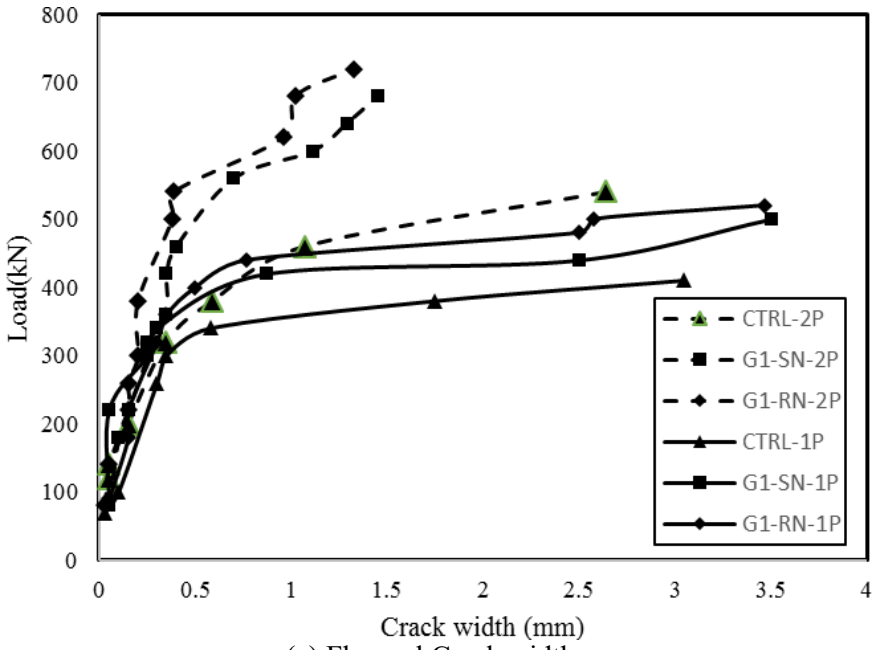

(a) Flexural Crack width.

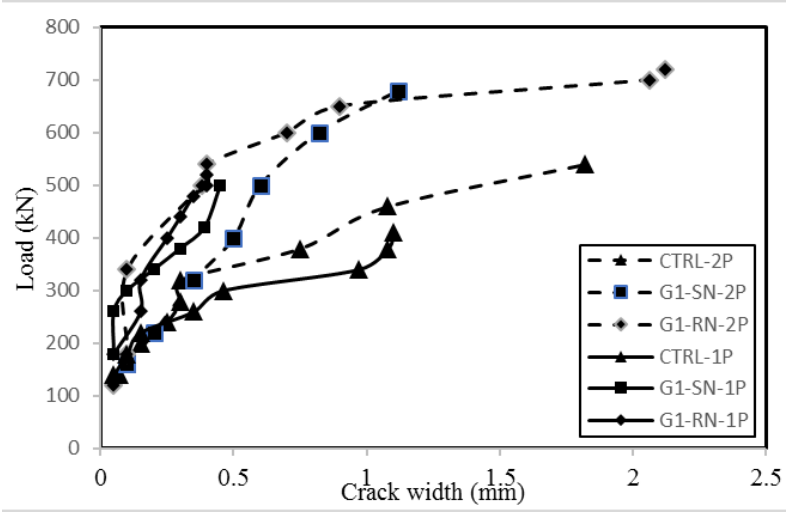

(b) Diagonal Crack width.

Fig. 9. Flexural and diagonal crack width.

3.4 Dissipated energy

The area under the load-deflection curve when stiffness is greater than zero was termed as the flexural toughness or the dissipated energy. It is a quantitive measure of the resistance of a member to distortions before failure. As a result, the member's energy output gradually decreases until failure [35]. With a calculated toughness of 3908 kN . mm, the reference CTRL-1P specimen has the lowest toughness of all the tested specimens, as shown in Figure (10). Because the SFC covers the majority of the strut area, the toughness of the specimen G1-SN-1P increased by 28% when steel fibers were used in the top layer. When it comes to specimens with two concentrated loads, the enhancement in required dissipation of energy to reach failure was more evident, as the flexural energy of the control specimen (CTRL-2P) was 4413 kN. mm, the energy required to cause failure in G1-SN-2P specimen increased by 143.7%. The toughness of deep beams improved noticeably when steel fiber concrete, or RPC, was used partially. This improvement was more recognized in the model of full arch, which yields more warnings prior to failure. The toughness ranged from (28-44) % for one point loading specimens to (144-188) % for two-point loading specimens. It was noticed that the toughness increased for one- and two- point loading when RPC

is used in place of SFC. The increments for the hybrid models G1-RN-1P and G1-RN-2P are 44% and 188.5%, respectively.

3.5 Ductility ratio

Ductility may be defined as the range of the ability of a member to resist inelastic deformation up to the maximum capacity [35], [36], [37]. A structural element with high value of ductility ratio could, in general, accommodate considerable amounts of deformations before being failed.

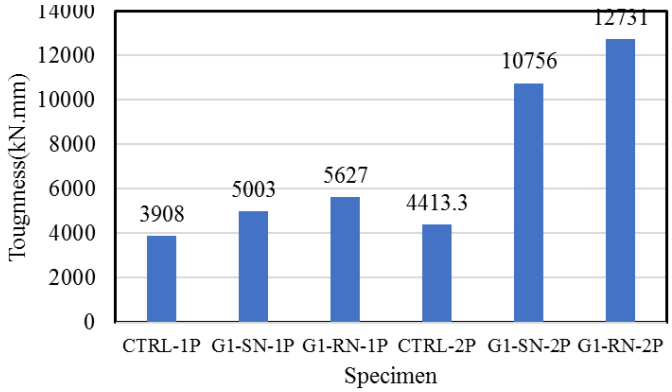

Fig 10 Toughness values

Several approaches were proposed when the value at which steel yields is not available. As illustrated in Figure 11, it can be computed using the quantity of the dissipated energy throughout the full regime of loading. The ductility ratio may be written as follows:

$$\mu = 0.5\left(\left({}^{E_{tot.}}/_{E_{el.}}\right) + 1\right) \quad (1)$$

$E_{tot.}$ is the area under the load-deflection curve (non-descending part) up to failure,

$E_{el.}$ is dissipated energy within the elastic stage (hatched area).

Fig. (12) presents the findings. In comparison to the control specimen, it was observed that incorporating SFC in the concrete of the top half of the beam specimens G1-SN-1P and G1-SN-2P results in enhancing their ductility by 6.6% and 32.5%, respectively. Comparing the RPC specimens with hybrid deep beam to the reference specimens, the ductility increased by 40.4% at the two-point loading of specimen G1-RN-2P and decreased by 9% at one point loading for specimen G1-RN-1P.

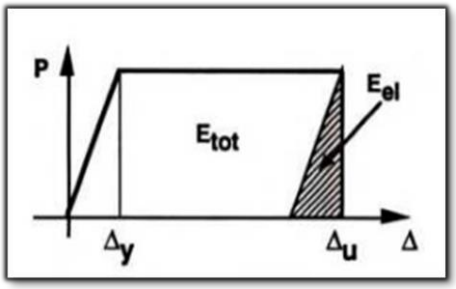

Fig. 11. Determination of ductility ratio [36].

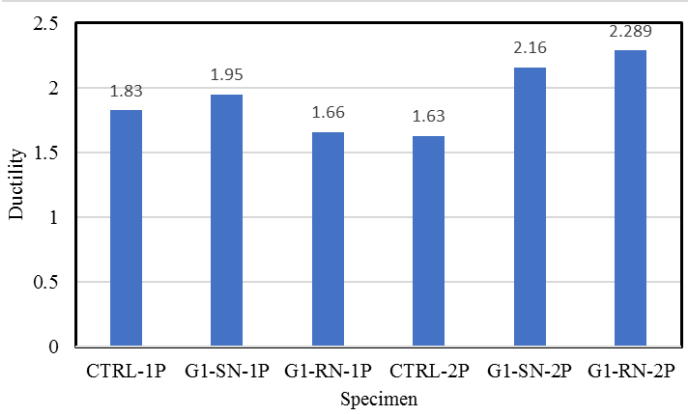

Fig. 12. Ductility values.

4 Conclusions

In the current work, a layered model based on using high performance concrete (HPC) at the top half of the section only has been considered. Six specimens were tested experimentally under static load up to failure. It is aimed to determine the range of improvement in the general performance due to use of steel fiber concrete (SFC) or reactive power concrete (RPC) at the top half of the deep beams. Moreover, the effect of loading configuration (one-point or two points) which considered implicitly the effect of the shear span-to- depth ratio (a/h) was considered. The main conclusions drawn from the results of the experimental work are listed below:

1. the hybrid model of deep beams composed partially with steel fiber concrete resulted in enhancement in failure loads by 22% and 27% in comparison to the control specimens, for the one-point (a/h=1.67) and two-points (a/h=1.2), respectively. For specimens composed of RPC, the corresponding enhancements are 28% and 34%, respectively.

2.Applying the load in several points rather than on point may result in significant enhancement in the structural performance and a better stress transfer. Regarding the failure load, it was noticed that applying the load in two points (a/h=1.2) rather than one point (a/h=1.67) led to enhancement by 32%, 37%, and 39% for the non-hybrid, hybrid with SFC at top layer, and hybrid with RPC at top layer.

3.It can be observed that using the RPC instead of SFC at the top layer of the hybrid sections resulted in slight enhancements in the failure load of 6% and 7%. This slight difference refers that the high-performance concrete (HPC) is used in the region at which the compression struts are developed to transfer compressions stresses only which can be resisted by SFC. This refers that the relatively lower cost SFC is efficient to develop the required resistance rather than using the highly cost RPC. However, this difference may increase with higher content of steel fibers.

4. For one-point and two-point loading systems, the flexural toughness of layered specimens with SFC at the top layer was increased by 28% and 144%, respectively, compared to the control specimens. The corresponding improvements were 44% and 188%, respectively, when RPC was used in place of SFC.

The hybrid model that was suggested led to a maximum increase in ductility of 7% and 40% for loading systems that involved one pint and two points, respectively.

5. Notable improvements were observed in the crack width, propagation, and mode of failure. The failure of spalling and crashing at the compression face was decreased by using a layered model. The rate at which cracks propagate and widen is significantly limited. The application of layered models resulted in a more ductile mode of failure.

Funding

This research did not receive any specific grant from funding agencies in the public, commercial, or not-for-profit sectors.

Conflicts of interest

The authors declare no known competing financial interests or personal relationships that could have influenced the work reported in this paper.

Author's contribution statement

Qasim M. Shakir: conceptualization of the paper. Project administration; Resources, the experimental investigation, reading reviewing the draft, editing of the final submitted version.

Hawraa. H. Hannon: The experimental investigation, Resources, writing the original draft, editing of the final submitted version.

References

[1] Committee ACI. ACI 318-19. ACI318-19 Committee, "318M-19 Build Code Requir Concr Comment 2019:628.

[2] Lafta YJ. Specification of Deep Beams Affect the Shear Strength Capacity 2016;8:56–68.

[3] Mattock AH. Design proposals for reinforced concrete corbels. J Prestress Concr Inst 1976;21:18–42.

[4] Alqarni AS, Albidah AS, Abadel AA. Shear performance of reinforced concrete deep beams using different coarse aggregates under the effect of elevated temperatures. Case Stud Constr Mater 2022;16:e01087. https://doi.org/10.1016/J.CSCM.2022.E01087.

[5] Dang TD, Tran DT, Nguyen-Minh L, Nassif AY. Shear resistant capacity of steel fibres reinforced concrete deep beams: An experimental investigation and a new prediction model. Structures 2021;33:2284–300. https://doi.org/10.1016/j.istruc.2021.05.091.

[6] Smarzewski P. Analysis of failure mechanics in hybrid fibre-reinforced high-performance concrete deep beams with and without openings. Materials (Basel) 2018;12. https://doi.org/10.3390/ma12010101.

[7] Patil PSS, Shaikh AN, Niranjan PBR. Experimental and Analytical Study on Reinforced Concrete Deep Beam 2013;3:45–52.

[8] Zhang JH, Li SS, Xie W, Guo YD. Experimental study on shear capacity of high strength reinforcement concrete deep beams with small shear span-depth ratio. Materials (Basel) 2020;13. https://doi.org/10.3390/ma13051218.

[9] Ma C, Xie C, Tuohuti A, Duan Y. Analysis of influencing factors on shear behavior of the reinforced concrete deep beams 2022;45.

[10] Dalvand A, Sharififard E, Omidinasab F. Experimental investigation of mechanical and dynamic impact properties of high strength cementitious composite containing micro steel and PP fibers. J Rehabil Civ Eng 2020;8:73–89. https://doi.org/10.22075/JRCE.2020.17480.1332.

[11] Razzaghi H, Madandoust R, Aghabarati H. Strength Assessment of Steel Fibre Reinforced Recycled Aggregate Concrete by Means of Correlation between Ultrasonic and Point Load Tests. J Rehabil Civ Eng 2022;10:79–92. https://doi.org/10.22075/JRCE.2021.21898.1456.

[12] Isojeh B, El-Zeghayar M, Vecchio FJ. Fatigue resistance of steel fiber-reinforced concrete deep beams. ACI Struct J 2017;114:1215–26. https://doi.org/10.14359/51700792.

[13] Sergio Garcia AP and RP. Shear Strength of Sand-Lightweight Concrete Deep Beams with Steel Fibers. ACI Struct J 2021;118. https://doi.org/10.14359/51729347.

[14] Manharawy MS, Mahmoud AA, El-Mahdy OO, El-Diasity MH. Experimental and numerical investigation of lightweight foamed reinforced concrete deep beams with steel fibers. Eng Struct 2022;260:114202.

https://doi.org/10.1016/J.ENGSTRUCT.2022.114202.

[15] Sagar Varma Sagi M, Lakavath C, Suriya Prakash S. Effect of steel fibers on the shear behavior of Self-Compacting reinforced concrete deep Beams: An experimental investigation and analytical model. Eng Struct 2022;269:114802. https://doi.org/10.1016/J.ENGSTRUCT.2022.114802.

[16] Concha N, Aratan JR, Derigay EM, Martin JM, Taneo RE. A hybrid neuro-swarm model for shear strength of steel fiber reinforced concrete deep beams. J Build Eng 2023;76:107340. https://doi.org/10.1016/J.JOBE.2023.107340.

[17] Hussain LN, Hamood MJ, Al-shaarbaf EA. The behavior of UHPC deep beam using the hybrid combination of steel and basalt fibers 2024;7:226–43.

[18] Khaksefidi S, Ghalehnovi M. Effect of reinforcement type on the tension stiffening model of ultra-high performance concrete (UHPC). J Rehabil Civ Eng 2020;8:72–86. https://doi.org/10.22075/JRCE.2020.19420.1368.

[19] Ahmadi N, Yazdandoust M, Yazdani M. Simultaneous Effect of Aggregate and Cement Matrix on the Performance of High Strength Concrete. J Rehabil Civ Eng 2021;9:26–39. https://doi.org/10.22075/jrce.2021.20803.1431.

[20] H. M. Fahmi, I. A.S AlShaarbaf ASA. Behavior of Reactive Powder Reinforced Concrete Deep Beams. MSc Thesis, Civ Eng Univ Kufa, 2018:1–22.

[21] Hasan MJ, Al-Shamaa MFK. Effect bubbles on the behavior of reinforced reactive powder concrete deep beams. Int J Civ Eng Technol 2018;9:592–602.

[22] Makki AP. DRF, Jassem APDAT, Jassem HAA. Non-Linear Analysis of Reactive Powder Concrete (Rpc) Deep Beams With Openings Strengthened By Cfrp. Al-Qadisiyah J Eng Sci 2019;11:176–96. https://doi.org/10.30772/qjes.v11i2.551.

[23] Muhaison S, Abd W, Alwan M. Behaviour of Reactive Powder Rectaingular Deep Beam With Shear Zone Opening Subjected To Repeated Load. J Eng Sustain Dev 2018;2018:77–94. https://doi.org/10.31272/jeasd.2018.1.7.

[24] Falah Hassan H. Behavior of Hybrid Deep Beams Containing Ultra High Performance and Conventional Concretes. Eng Technol J 2015;33:30–50. https://doi.org/10.30684/etj.33.1a.3.

[25] Hassan SA, Ali MK. Behavior of Hybrid Reinforced Concrete Deep Beams With Web Openings Under Repeated Loading. J Eng Sustain Dev 2019;23:52–75. https://doi.org/10.31272/jeasd.23.4.4.

[26] Ma K, Qi T, Liu H, Wang H. Shear Behavior of Hybrid Fiber Reinforced Concrete Deep Beams. Materials (Basel) 2018;11:2023. https://doi.org/10.3390/ma11102023.

[27] Mhalhal JM, Al-Gasham TS, Abid SR. Tests on reinforced concrete deep beams with different web reinforcement types. IOP Conf Ser Mater Sci Eng 2020;988. https://doi.org/10.1088/1757-899X/988/1/012032.

[28] Sada MJ, Resan SF. Shear Performance of Hybrid Concrete Deep Beams of Trapezoidal Section. IOP Conf Ser Mater Sci Eng 2021;1067:012015. https://doi.org/10.1088/1757-899x/1067/1/012015.

[29] Shakir QM, Hanoon HK. BEHAVIOR OF HIGH-PERFORMANCE REINFORCED ARCHED- HYBRID SELF-COMPACTING CONCRETE DEEP BEAMS. J Eng Sci Technol 2023;18:792–813.

[30] Mohammed Shakir Q, Hannon HK. a Novel Hybrid Model of Reinforced Concrete Deep Beams With Curved Hybridization. J Teknol 2023;85:31–9. https://doi.org/10.11113/jurnalteknologi.v85.18703.

[31] Shakir QM, Hanoon HK. New models for reinforced concrete precast hybrid deep beams under static loads with curved hybridization. Structures 2023;54:1007–25. https://doi.org/10.1016/j.istruc.2023.05.084.

[32] Shakir QM, Alghazali AF. Effect of the arching action on the behavior of the RC precast concrete deep beams: comparison between several hybrid models. J Build Pathol Rehabil 2024;9. https://doi.org/10.1007/s41024-023-00377-0.

[33] Shakir QM, Alghazali AF. Hybrid Curved Precast Deep Beams Composed Partially from Concrete Made with Recycled Concrete Aggregate. E3S Web Conf 2023;427:1–8. https://doi.org/10.1051/e3sconf/202342702025.

[34] Shakir QM, Alghazali AF. New Model of Eco-Friendly Hybrid Deep Beams With Wastes of Crushed Concrete. J Teknol 2023;85:145–54. https://doi.org/10.11113/jurnalteknologi.v85.20431.

[35] Shakir QM, Abd BB. Retrofitting of self compacting rc half joints with internal deficiencies by cfrp fabrics. J Teknol 2020;82:49–62. https://doi.org/10.11113/jurnalteknologi.v82.14416.

[36] Taerwe L. Non-Metallic (FRP) Reinforcement for Concrete Structures. CRC Press; 2004. https://doi.org/10.1201/9781482271621.

[37] Rakhshanimehr M, Esfahani MR, Kianoush MR, Mohammadzadeh BA, Mousavi SR. Flexural ductility of reinforced concrete beams with lap-spliced bars. Can J Civ Eng 2014;41:594–604. https://doi.org/10.1139/cjce-2013-0074.